MICROSTRUCTURAL STABILITY AND ORIENTATION RELATIONSHIPS OF DIRECTIONALLY SOLIDIFIED Al_2O_3-$Er_3Al_5O_{12}$-ZrO_2 EUTECTIC CERAMICS UP TO 1600ºC.

M. C. Mesa*, S. Serrano-Zabaleta, P. B. Oliete, A. Larrea

Instituto de Ciencia de Materiales de Aragón, CSIC–Universidad de Zaragoza,

María de Luna 3, 50018 Zaragoza, Spain.

* Corresponding author: M. C. Mesa Tel: +34 876 555 223; Fax: +34 976 761 957

E-mail adresses: mcmesa@unizar.es (M. C. Mesa); zabaleta@unizar.es (S. Serrano-Zabaleta); poliete@unizar.es (P.B. Oliete); alarrea@unizar.es (A. Larrea)

ABSTRACT

Al_2O_3-$Er_3Al_5O_{12}$-ZrO_2 eutectic ceramic rods were directionally solidified using the laser floating zone method at different growth rates, 25, 350 and 1200 mm/h. The microstructure obtained, in terms of both morphology and phase size, was strongly dependent on the growth rate. However, electron backscatter diffraction experiments showed that the growth directions were the same for all the processing rates, $[0001]_{Al2O3}//[100]_{EAG}//[100]_{ZrO2}$. The microstructural stability was investigated up to 1600ºC as a function of the growth rate. Ceramics with the largest phase size presented high stability, their microstructure remaining substantially unchanged at the highest annealing temperature for 100 hours. Eutectics processed at higher growth rates and with a finer microstructure showed coarsening after heat treatments. The sample grown at 350 mm/h coarsened at 1450ºC whereas the eutectic solidified at 1200 mm/h thickened at 1400ºC. The growth directions remain unaffected for all growth rates. The mechanisms of microstructural coarsening were investigated.

Keywords: $Al_2O_3/Er_3Al_5O_{12}/ZrO_2$; Directionally solidified eutectic ceramics; Microstructural stability; Coarsening; Orientation relationships.

1. INTRODUCTION

Directionally solidified eutectic ceramics (DSEC) are materials constituted by two or more eutectic phases whose microstructure can be controlled by the solidification conditions [1]. Most of the properties of the eutectics depend on the shape and size of the phases. The relationship between microstructure and properties allows the characteristics of DSEC to be controlled by the processing parameters.

Among DSEC, those based on Al_2O_3 have been the subject of a large number of studies because of their outstanding mechanical properties up to temperatures very close to the melting point, and an excellent microstructural and chemical stability [2], which make them promising materials for structural applications at high temperatures [2, 3]. Most of the studies found in the literature have focused on eutectics of the $Al_2O_3/Y_2O_3/ZrO_2$ system [4-7]. Mechanical properties have been reported to depend strongly on the microstructural size, showing a significant improvement when the size of the eutectic phase is reduced [8]. Outstanding flexural strength close to 5 GPa was obtained for the Al_2O_3-$Y_3Al_5O_{12}$-ZrO_2 ternary eutectic (AYZ)' with nanometric phases due to the high rates used in processing [9]. In addition, high strength retentions up to 1900K were found for the Al_2O_3-$Y_3Al_5O_{12}$ binary eutectic (AY) [8].

Recently, other Al_2O_3-based DSEC including rare earth oxides in their eutectic composition have been studied. The incorporation of rare earth ions allows the field of applications of these materials to be extended. In addition to structural applications at high temperatures, they can be used in functional applications such as selective thermal emitters in thermophotovoltaic devices [10]. We should note that both applications

implicate high operating temperatures. When the materials are exposed to high temperatures for long periods of time, microstructural coarsening may appear, producing the degradation of the material performance. Martinez-Fernandez *et al.* studied the high temperature creep deformation of directionally solidified $Al_2O_3/Er_3Al_5O_{12}$. They reported that the material presented a very high creep resistance, comparable to c-axis sapphire, concluding that creep deformation was diffusion controlled.[11] In fact, they limited the study of creep curves to temperatures below 1500 ºC because of the microstructural evolution of the samples. Then, Mazerolles and co-workers studied the microstructure, interfaces and high temperature creep behaviour of Al_2O_3-Ln_2O_3 (Ln=Gd, Er, Y) DSEC.[12,13] They pointed out that the absence of intermediate phases at the interfaces and the crystallographic orientation relationships between phases give rise to a strong cohesion between components. They also confirmed that deformation climb process was controlled by bulk diffusion. The remarkable creep resistance of these materials would be related to the quality of these interfaces. Furthermore, they also extended their study to ternary eutectics with the addition of a toughening phase (ZrO_2) Despite the significant interest in the performance of these materials at elevated temperature, the thermal microstructural stability of Al_2O_3-based DSEC has been scarcely investigated. Very few microstructural stability studies of the binary Al_2O_3-$Y_3Al_5O_{12}$, Al_2O_3-$Er_3Al_5O_{12}$ and Al_2O_3-$GdAlO_3$ eutectics [14-18] can be found in the literature and, to our knowledge, none related to any ternary DSEC.

The aim of this paper is to study the microstructural stability of the Al_2O_3-$Er_3Al_5O_{12}$-ZrO_2 (AEZ) ternary eutectic at a wide range of temperatures, up to 1600ºC. Al_2O_3-$Er_3Al_5O_{12}$-ZrO_2 eutectic rods were grown using the laser-heated floating zone method (LHFZ) and at different growth rates in order to investigate the influence of the

microstructure on thermal stability. For this purpose we studied, on the one hand, the evolution of the eutectic interspacing and interfacial area as a function of the annealing treatment using Field Emission Scanning Electron Microscopy (FESEM). On the other hand, we also determined by Electron Backscattering Diffraction (EBSD) the growth directions and orientation relationships of the as-grown eutectic phases and after the most extreme annealing was applied (1600ºC for 100h).

2. MATERIALS AND EXPERIMENTAL DETAILS

Eutectic rods of Al_2O_3-$Er_3Al_5O_{12}$-ZrO_2 were directionally solidified by the LHFZ method. Ceramics were prepared with a mixture of commercial powders of Er_2O_3 (Aldrich, 99.99%), Al_2O_3 (Sigma-Aldrich, 99.99%) and ZrO_2 (Aldrich, 99%) in the ternary eutectic composition (65.9 mol% Al_2O_3, 15.5 mol% Er_2O_3, 18.6 mol% ZrO_2) [19]. Precursor rods were prepared by cold isostatic pressing of the powder for 3 min at 200 MPa. The obtained rods were sintered in a furnace at 1500ºC for 12 hours. The final precursor rods had a typical diameter of 2.5 mm.

Eutectic rods were obtained by directional solidification with the LHFZ method using a continuous wave CO_2 laser at 25 mm/h, 350 mm/h and 1200 mm/h growth rates. To eliminate the precursor porosity, different densification stages were applied at a low growth rate (100-250 mm/h). The final directional solidification was always performed with the grown crystal travelling downwards and without rotation of the crystal or the precursor. Processing was performed in a nitrogen atmosphere with a slight overpressure of 0.1-0.25 bar respect to ambient pressure [20] in order to avoid the presence of voids in the solidified rods. The final processed rods had typical diameter values of 1-1.5 mm. From now on, the different processed rods will be referred to using the acronym AEZx where x is the solidification rate.

For the microstructural stability study, annealings were performed in air at temperatures ranging from 1350ºC to 1600ºC in steps of 50ºC, for fixed periods of 25 h, 50 h and 100 h. The heating and cooling rates were 3ºC/min and 5ºC/min, respectively.

Microstructural characterization was performed in polished transverse and longitudinal cross-sections of the as-grown and heat-treated rods by means of back-scattered electron images obtained in a Merlin Field Emission Scanning Electron Microscopy (FESEM) from Carl Zeiss (Germany). The energy of the incident electrons was 0.75 keV and we used an in-lens detector equipped with a filtering grid to reject electrons with energy lower than 0.72 keV in order to increase the contrast between the different phases. Specimens for this characterization were prepared using conventional metallographic methods. The eutectic interspacing, λ, and the amount of interfacial area per unit volume or surface density, S_v, in both as-grown and heat-treated rods, were measured using linear interception methods [21]. Due to the complex microstructure in these eutectics consisting of three phases in irregular arrays, the interspacing was defined as the length between two consecutive EAG crystals. It was calculated from transverse cross-section micrographs using a maximum of twenty randomly drawn lines containing at least four λ. The surface density was obtained from micrographs of the transverse and longitudinal cross-sections using the number of interphase intersections in a counting circle, in order to avoid texture effects.

In order to determine the growth directions and orientation relationships between phases, for the as-grown material and after the most extreme ageing treatment (100 h at 1600ºC), EBSD experiments were performed in transverse cross-sections using the FESEM equipment mentioned above. The accelerating voltage was of 10-15 kV with 1 nA probe current. The specimens were tilted at 70º, at distances of 14.5-17.5 mm from the pole piece and 178.5 mm from the EBSD detector (HKL, Oxford Instruments, UK),

which consisted of a CCD camera set at resolution of 514 x 384 using 4x4 binning. Two Kikuchi patterns were acquired (90-100 ms of acquisition time) every 0.02-0.15 μm, averaged out and automatically indexed (7 bands out of 50 reflectors) to determine the crystal orientation at every point [22]. In order to avoid charge accumulation on the sample surface due to the AEZ being an electrical insulator, the specimen was not coated but instead an N_2 micro jet was pointed towards the surface of the sample during the experiments for charge compensation. [23]

The specimen preparation for EBSD experiments required a special method because the electron diffraction patterns are generated on a very thin surface layer (~40 nm thick) that has to be free of strains [24]. It consisted of polishing transverse cross-sections of the samples in progressive steps using Struers LaboPol-4 automated polisher, first with SiC paper (15 μm and 10 μm particle size with the polishing wheel rotating at 40 rpm and under a load of 2.5 N), subsequently with diamond paste (3 μm and 1 μm particle size, 120 rpm, 2.5 N) and finally with colloidal silica (0.04 μm particle size,100 rpm, 2.5 N) for 15 min.

3. RESULTS AND DISCUSSION

3.1. Microstructural stability and coarsening kinetics

The FESEM micrograph analysis of samples with different heating treatments was used to study the evolution of the microstructure with temperature and time. From this study we quantified the coarsening of the eutectic phases in order to investigate coarsening kinetics.

Figure 1 shows electron images of transverse cross-sections of the as-grown eutectic rods processed at (a) 25 mm/h, (b) 350 mm/h and (c) 1200 mm/h. Three different phases can be observed for all the growth rates, Al_2O_3 (dark phase), $Er_3Al_5O_{12}$

(EAG, grey phase) and cubic Er_2O_3-stabilized ZrO_2 (ESZ, light phase), all of them identified by energy dispersive spectrometry (EDS). The erbia content in the ESZ phase had been previously determined by X-ray diffraction and reported to be 15 mol% [25]. The experimental volume fractions of 39 ± 1%, 40 ± 1%, and 21 ± 1%, obtained from image analysis for Al_2O_3, EAG, and ESZ, respectively, were roughly close to the volume fractions calculated using the eutectic composition (42 ± 2%, 38 ± 2%, and 20 ± 2%, respectively) [25].

As can be seen, both the morphology and the phase size depend on the growth rate. For samples grown at 25 mm/h the microstructure consisted of a geometrical array of EAG prismatic columnar crystals and columnar domains formed by an Al_2O_3-ESZ interpenetrated network (figure 1 (a)). For samples processed at 350 mm/h the microstructure was a three-dimensional irregular interpenetrated microstructure of the three eutectic phases (figure 1 (b)). Finally, the eutectic rods grown at 1200 mm/h showed a fibrillar microstructure consisting of bundles of nano-sized sapphire three-fold shaped rods aligned in the growth direction (figure 1(c)), embedded in an EAG matrix with the ESZ phase placed at the EAG-Al_2O_3 interphases. For all the processing rates, the grains were elongated along the growth direction (figure 2(a)). In addition, the size of the eutectic phases decreased with the processing rate. The eutectic interspacing, λ, decreased from 4.8 μm for AEZ25 to 300 nm for AEZ1200. Table 1 shows the eutectic interspacing determined in the as-grown eutectic rods for all the growth rates.

The microstructure of the ceramics was investigated after the different heat treatments. Figure 1 shows the transverse cross-sections of AEZ25 (d) and (g), AEZ350 (e) and (h), and AEZ1200 (f) and (i), after annealing at 1450ºC for 100h and after annealing at 1600ºC for 100h, respectively. In addition, table 1 presents the interspacing

obtained after the most extreme annealing for rods grown at 25 mm/h, 350 mm/h and 1200 mm/h.

The eutectic processed at 25 mm/h and with the largest phase size presented a high thermal microstructural stability. The microstructure of AEZ25 remained substantially unchanged even for the highest annealing temperature and the longest time, 1600ºC for 100h. The only variations observed were a slight thickening of the ESZ phase after annealing at 1600°C for 100h probably due to the submicrometric size of the ESZ phase, and a variation of EAG columnar crystal shape, becoming more rounded after the highest annealing temperature and the longest time. The eutectic interspacing (λ) remained constant for all the heat treatments (see table 1). High thermal microstructural stability has been also reported in some binary DSEC, with similar size of the phases as in Al_2O_3-$Er_3Al_5O_{12}$ eutectics processed at 25 mm/h [12] and Al_2O_3-$Y_3Al_5O_{12}$, Al_2O_3-$Er_3Al_5O_{12}$ and Al_2O_3-$GdAlO_3$ eutectics processed at 5 mm/h [14, 15].

However, for AEZ samples grown at higher rates and, therefore, with finer microstructures, significant coarsening was observed. The coarsening was homogeneous throughout the sample cross-sections and there was no evidence of exaggerated localized coarsening, contrary to that observed in binary Al_2O_3-$Er_3Al_5O_{12}$ [16] and Al_2O_3-$Y_3Al_5O_{12}$ [18, 26] eutectics.

In the case of AEZ350 the microstructure was invariable up to 1400ºC. After annealing at 1400ºC for 100h, spheroidization of the eutectic phases was observed. When samples were annealed at higher temperatures, the microstructure coarsened. Finally, AEZ1200 was the eutectic with the lowest thermal microstructural stability, with coarsening being observed at lower temperatures. After annealing at 1350ºC, rounding of the eutectic phases and thickening of the ESZ phase were observed. The ESZ phase was placed linking close Al_2O_3 crystals. At 1400ºC and above, coarsening

appeared for the rest of the phases. Figure 2 shows the longitudinal cross-section of the as-grown eutectic AEZ1200 (a) and after annealing at 1600ºC for 100h (b). The elongation of the grains along the growth direction disappeared when the phases coarsened, the grains becoming equiaxial.

The eutectic interspacing in AEZ350 and AEZ1200 samples as a function of time at annealing temperatures is presented in figure 3. The major coarsening of the eutectic with the smallest phase size, AEZ1200, is noticeable. In particular, in this eutectic, λ increased from 0.3±0.03 μm to 2.1±0.3 μm after annealing at 1600ºC for 100h.

In addition to eutectic interspacing, the surface density variation with heat-treatments was also investigated. Table 2 shows the S_v values obtained from transverse and longitudinal cross-sections for AEZ25, AEZ350 and AEZ1200 in as-grown and annealed rods. Note that the S_v values obtained in the as-grown rods increased with the growth rate, due to the reduction of the eutectic phase size which results in a higher number of interphases. However, for the more extreme heat-treatment, S_v values were very similar for all the rods because of the major coarsening observed in the samples with finer microstructures. We can also observe in table 2 that the S_v obtained from longitudinal cross-section micrographs is slightly lower for all the growth rates due to the grain elongation along the growth direction. In the case of AEZ1200 after the heat-treatment at 1600ºC for 100h, the elongation of the grains along the growth direction practically disappeared (figure 2 (b)) and, as a consequence, S_v calculated in the transverse and longitudinal cross-sections are similar. Finally it is emphasized that although λ did not show variations in AEZ25, the surface density showed a slight reduction after annealing at 1600º C because of the thickening of the ESZ phase.

Figure 4 shows the surface density as a function of the annealing time for different temperatures of samples AEZ350 (a) and AEZ1200 (b). We can observe that in both

cases S_v significantly decreased with increasing temperature and time, with the surface density reduction being especially evident in the rods grown at 1200 mm/h.

The lower thermal microstructural stability of the AEZ350 and AEZ1200 eutectics compared with that of AEZ25 is due to the smaller size of the eutectic phases. The driving force of eutectic microstructure coarsening is the reduction of the interfacial energy [27, 28]. The smaller the phase size, the microstructure involves a greater number of interfaces and, hence, the higher the interphase energy. The coarsening of the finer eutectic microstructures produces a reduction in the interfacial area (see figure 4) and thus, a decrease in the energy of the system. In addition, the smaller phase size favoured coarsening at elevated temperatures as the large number of interfaces in AEZ350 and AEZ1200 enhanced the diffusion process.

Analysis of the microstructure size as a function of time allows more information about coarsening kinetics to be obtained. From the phase size dependence with time it is possible to establish the process that controls the phenomenon of phase thickening [29]. For eutectic microstructures, where the volume fraction of the eutectic phases remains constant, the rate-controlling process can be determined by obtaining n from the following equation [27]

$$2/S_v = c \cdot t^{1/n} \qquad (1)$$

where c and n are constants. If the process is diffusion-controlled, n is equal to 3 or 4 (3 for diffusion through volume [28, 30] and 4 for diffusion through the grain boundary [31, 32]), while if the process which controls coarsening is the dissolution of atoms from one phase to the other phase, n is equal to 2 [27].

Therefore, to determine the rate-controlling process in AEZ eutectic coarsening, $\ln(2/S_v)$ was plotted vs $\ln(t)$ and the n value calculated from the slope. For both eutectics that presented coarsening, AEZ350 and AEZ1200, n was between 3 and 4,

indicating that the coarsening in AEZ is controlled by diffusion rather than by interface reaction (n=2). Non-integer coarsening exponents in coarsening processes have been previously reported [33] and associated to a combination of diffusion paths (bulk and interfacial). The coarsening rate will be governed by the diffusion rate of the slowest-moving species.

The activation energy of the coarsening, Q, could also be calculated from the surface density variation, using the same procedure as Park et al. [17]. From the Arrhenius law, logarithm of $1/S_v$-$1/S_0$ versus 1/T was plotted (being S_0 the surface density of the as-grown eutectic samples and T the annealing temperature). From the slope of the Arrhenius plots the Q-values for AEZ350 and AEZ1200 were determined. In AEZ350 the obtained Q-values were (259±49) kJ/mol and (288±73) kJ/mol, for transverse and longitudinal cross-sections, respectively. In the case of AEZ1200, the calculated Q-values were (350±42) kJ/mol and (319±55) kJ/mol, for transverse and longitudinal cross-sections, respectively. The obtained activation energy values were very similar in both eutectics and practically independent on the cross-section analysed, ~ 300 kJ/mol. In addition, the activation energy obtained for the Al_2O_3-$Er_3Al_5O_{12}$-ZrO_2 ternary eutectic was similar to the activation energy estimated for Al_2O_3-$Er_3Al_5O_{12}$ [16] and Al_2O_3-$Y_3Al_5O_{12}$ eutectics [17]. In the case of Al_2O_3-$Er_3Al_5O_{12}$ eutectics, the activation energy was estimated in samples grown at 350 mm/h ((284±54) kJ/mol and (227±73) kJ/mol, for transverse and longitudinal cross-sections, respectively) and in samples grown at 750 mm/h ((205±54) kJ/mol and (252±77) kJ/mol, for transverse and longitudinal cross-sections, respectively). In Al_2O_3-$Y_3Al_5O_{12}$ eutectics, the Q-value was obtained for the surface (262±42 kJ/mol) and the longitudinal-section areas (308±103 kJ/mol).

In AEZ eutectics, Al^{3+}, O^{2-}, Er^{3+} and Zr^{4+} ions are the species involved in the diffusion process. To determine which are the ions controlling the rate of coarsening, it is necessary to know the activation energy for the diffusion of these ions through the eutectic phases, Al_2O_3, EAG and ESZ, and the corresponding interfaces. Unfortunately, there are no available data on activation energies for all the species in the three eutectic phases of AEZ. For diffusion of Er^{3+} ions through Al_2O_3 and ESZ, and for diffusion of Al^{3+}, O^{2-}, Er^{3+} and Zr^{4+} ions through EAG no data were found and so the diffusion of Al^{3+}, O^{2-}, Y^{3+}, Zr^{4+} ions through Al_2O_3, YAG and Y_2O_3-stabilised cubic zirconia was considered. The only available data were the diffusion activation energies for Al^{3+} through Al_2O_3 ([477 kJ/mol [34]-[35]); Y^{3+} through Al_2O_3 (295 kJ/mol [36] and 335 kJ/mol [37]), O^{2-} through Al_2O_3 (615-786 kJ/mol[35], [38]) and O^{2-} through YAG (304-325 kJ/mol [39-41]). No significant differences are expected in the activation energy value for Er^{3+} diffusion in bulk Al_2O_3 with respect to the reported values for Y^{3+} diffusion. All studied trivalent impurities in alumina diffuse quite rapidly and the Q-values reported are very similar regardless of the ion in question. [36, 42]

The activation energy obtained from the coarsening study is close to the activation energies for diffusion of O^{2-} through YAG and Y^{3+} through Al_2O_3. O^{2-} diffusion is required to maintain charge neutrality. However, as the three eutectic phases are oxygen compounds, only short range diffusion is needed in the oxygen sublattice [18]. It is more probable that the rate limiting ion in the coarsening of this eutectic is the erbium ion.

Therefore, we tentatively attribute the rate-controlling mechanism for coarsening in AEZ eutectics to the diffusion of Er^{3+} ions through Al_2O_3. Similar results were reported for Al_2O_3-$Er_3Al_5O_{12}$ [16] and Al_2O_3-$Y_3Al_5O_{12}$ eutectics [17]. In the Al_2O_3-

$Y_3Al_5O_{12}$ eutectic, interphase diffusion of Y^{3+} has also been proposed as the process which limits the rate of thickening [18].

Although no microstructural stability investigations were found in the literature for directionally solidified ternary Al_2O_3-based eutectics, a study of sintered ceramics with the AYZ eutectic composition has recently been reported [43]. Heat treatments at 1500ºC for 100 h in samples with a phase size similar to AEZ350 produced significantly greater coarsening than that observed in our samples. Therefore, microstructural coarsening is not only dependent on the constituent phases of the material and its size. The nature of the interphases is also an important factor, the eutectic interphases being more resistant to the coarsening than interphases obtained by sintering.

3.2. Growth directions and orientation relationships

EBSD experiments were performed on transverse cross-sections of the as-grown materials solidified at each growth rate, 25, 350 and 1200 mm/h, with the aim of determining the growth directions and orientation relationships between phases prior to annealing. Afterwards, transverse cross-sections of the samples whose microstructure resulted most altered by the annealing, i.e., those samples that underwent 100 h of heat treatment at 1600ºC, again for all growth rates, were also analyzed by means of EBSD in an attempt to get more information about the coarsening mechanism.

Those experiments consisted of scanning several areas of the specimen surface and acquiring Kikuchi patterns over numerous equidistant points forming a grid. This Orientation Imaging Microscopy (OIM) technique provides us with online information on the crystal orientation of each phase, which is registered and may be refined in subsequent offline analysis of the data and expressed in pole figures and orientation

maps, among other analytic and graphic tools included in the EBSD analysis software. [22]. EBSD technique is a powerful tool that has been successfully applied to the study of several DSEC microstructures. [44-46] This technique allows getting the orientation relationships and the interfaces of large areas with an angular accuracy below 0.5º.

3.2.1. As-grown

Figure 5 shows an orientation map obtained for the as-grown AEZ25 sample. Several maps were collected from the same cross-section, showing identical results. In an orientation map, the colour or grey level of each pixel is unequivocally related to the crystal orientation of the sample at the corresponding point over the specimen surface. In figure 5, only 3 hues are found, one for each phase. This means that AEZ25 is highly textured, and that each phase behaves as a single crystal throughout all the sample cross-section, in spite of the complex microstructural configuration. Neither EAG prismatic columns nor ESZ clusters seem to be in touch with each other; nonetheless they present the very same crystal orientations throughout the whole transverse cross-section. This fact can only be understood considering that strong interfaces with well-defined orientations relationships are formed in the eutectic. In addition, unlike other directionally solidified eutectics [47], AEZ seems not to be made up of several eutectic grains, but only one crystal orientation for each phase was found within the whole transverse cross-section.

Experimental pole figures showing the crystal orientation of each phase in the area depicted in figure 5 are displayed in figure 6. The growth directions are crystallographic directions close to the rod axis. Since the pole figures have been acquired over the transverse cross-section, growth directions may be recognized for being poles very close to the stereogram centre. In this case, the growth directions are

$[100]_{EAG}//[100]_{ESZ}//[0001]_{Al2O3}$. Identical growth directions of the eutectic phases were observed from XRD experiments in samples of this same Al_2O_3-$Er_3Al_5O_{12}$-ZrO_2 ternary eutectic but processed by the Bridgman technique at 30 mm/h [19]. The possible interface planes, if there were any, would be discerned among other crystal directions for being poles in each phase parallel to each other and approximately perpendicular to the growth direction; thus, poles close to the outline of the stereogram. In the present case, a perfect parallelism between $(010)_{ESZ}//(10\bar{1}\ 0)_{Al2O3}$ is observed, as shown in figure 6. However, the morphology of the microstructure in this case does not guarantee that the interfaces between the ESZ and the Al_2O_3 are indeed faceted and therefore, there might not be well-defined interface planes. Pole figures including higher Miller index planes (including the sapphire R-plane) than the ones in figure 6 were unsuccessfully examined in an attempt to find other parallelisms between phases, in particular between EAG and Al_2O_3. In all events, the OR between phases for the as-grown AEZ25 specimen is:

$[100]_{EAG}//[100]_{ESZ}//[0001]_{Al2O3}$ (growth directions)

$(010)_{ESZ}//(10\bar{1}\ 0)_{Al2O3}$ and $(011)_{EAG}$ forming 4.5^0 with $(10\bar{1}\ 0)_{Al2O3}$

We would like also to point out that the Al_2O_3 growth direction we observed is 90º from that reported by Mazerolles *et al*. in the similar Al_2O_3-$Y_3Al_5O_{12}$-ZrO_2 eutectic. [46] Our growth directions are their interfacial planes. Figure 7 shows the orientation map for the as-grown AEZ solidified at 350 mm/h. Again EAG and Al_2O_3 phases behave as single crystals, whereas some scattering is found for the ESZ. The growth directions are the same as for the as-grown AEZ25. The parallelism $(010)>_{ESZ}//(10\bar{1}\ 0)_{Al2O3}$ is also found in this case, but the EAG phase has rotated around its growth direction in comparison

with AEZ25. The OR between the phases throughout the AEZ350 cross-section being studied is:

$[100]_{EAG}//[100]_{ESZ}//[0001]_{Al2O3}$ (growth directions)

$(010)_{ESZ}//(10\bar{1}\,0)_{Al2O3}$ and $(011)_{EAG}$ forming 19.5^0 with $(10\bar{1}\,0)_{Al2O3}$

For the as-grown AEZ1200 the ESZ scattering is greater than for the previous cases, while the growth directions and the parallelism $(010)_{ESZ}//(10\bar{1}\,0)_{Al2O3}$ remain in spite of the change in the microstructural type (figure 8 (a)). The OR in this case is nearly the same as that obtained for the AEZ25 sample:

$[100]_{EAG}//[100]_{ESZ}//[0001]_{Al2O3}$ (growth directions)

$(010)_{ESZ}//(10\bar{1}\,0)_{Al2O3}$ and $(011)_{EAG}$ forming 5^0 with $(10\bar{1}\,0)_{Al2O3}$

Two other transverse cross-section specimens of AEZ25 and AEZ1200 obtained from different rods were also analyzed. In these cases, different angles between the $(011)_{EAG}$ and $(10\bar{1}0)_{Al2O3}$ planes were obtained. Thus the angle between the $(010)_{EAG}$ and $(10\bar{1}\,0)_{Al2O3}$ planes probably is not an intrinsic OR characteristic of the AEZ eutectics. Although it remains constant throughout all of the transverse cross-sections analyzed, it changes for different rods. Besides, it is noticeable that ESZ and Al_2O_3 phases always maintain a fixed OR as they grow, regardless of the very dissimilar microstructure of the samples processed at different growth rates. It might be inferred that, as Al_2O_3 is the major phase and also presents the higher entropy of fusion and growth anisotropy, it is the phase that controls the solidification whereas the ESZ phase accommodates to the Al_2O_3 crystal orientation [1]. Although EAG always grows along the [100] direction, it seems that it cannot accommodate a fixed OR with respect to the other two phases.

3.2.2. Annealed samples

The effect of the 100 h heat treatment at 1600 ºC on the AEZ25 is almost negligible in relation to the growth directions, which remain invariant, and to the little or non-observed orientation dispersion. No significant differences in comparison with the as-grown sample were found, apart from the angle formed between $(011)_{EAG}$ and $(10\bar{1}0)_{Al2O3}$, which is now 25º. Since the after-annealing specimen on which the EBSD experiments were performed was not the same as for the as-grown EBSD experiments, this change in the OR is not necessarily a reorientation caused by the annealing, but instead, the annealed rod could have shown this OR before the heat treatment. These experimental findings are consistent with the high thermal stability of AEZ25, embodied in the low variation of the eutectic interspacing and surface density described in section 3.1.

Ageing neither affects the growth directions nor the parallelism between the ESZ and Al_2O_3 phases of AEZ350. Only the orientation scattering increases slightly for the EAG and Al_2O_3 phases and more significantly for the ESZ. The angle determined this time between $(011)_{EAG}$ and $(10\bar{1}0)_{Al2O3}$ was 13º. Finally, experiments on AEZ1200 after heat treatment showed a notorious increase in orientation scattering for all the phases (figure 8 (b)), while the growth directions still remain unchanged. For the first time, $(010)_{ESZ}$ and $(10\bar{1}0)_{Al2O3}$ appeared 28º average misoriented, while the angle between $(011)_{EAG}$ and $(10\bar{1}0)_{Al2O3}$ was 17º. As a consequence the new OR was:

$[100]_{EAG}//[100]_{ESZ}//[0001]_{Al2O3}$ (growth directions)

$(010)_{ESZ}$ forming 28º with $(10\bar{1}0)_{Al2O3}$ and $(011)_{EAG}$ forming 17^0 with $(10\bar{1}0)_{Al2O3}$

From these experiments we can conclude that the crystallographic growth directions remain unaltered after the annealing treatments. Regarding the other parallelism defining the full OR, it is not easy to discriminate whether the small variations observed

are produced by the annealing, or by the fact that we are analyzing different specimens. Our feeling is that they were not due to annealing. In fact, the coarsening mechanism, as established in section 3.1, is a mixed volumetric and interfacial atom diffusion from the small grains to the larger ones in order to reduce the interfacial energy. In this way, the large grains that coarsen should not change their crystallographic orientation. These results are also consistent with the experiments of Graham and Kraft that did not observe any changes in the crystallographic or interface relationships during the thickening process of Al-$CuAl_2$ lamellar eutectics [27].

4. CONCLUSIONS

In this paper the microstructural thermal stability and the orientation relationships of the directionally solidified AEZ eutectics up to 1600ºC were investigated. The study was performed in eutectic rods processed at three processing growth rates in order to achieve different microstructures. As was expected, the microstructural thermal stability strongly depended on the microstructure. The microstructure of the eutectic grown at the lower rate (25 mm/h), with the largest phases, remained practically invariable even after the most extreme heat-treatment. For the eutectics processed at higher rates (350 and 1200 mm/h), with smaller phase size, the microstructure coarsened. In the finer microstructure, coarsening occurred at lower temperatures. AEZ350 coarsened at annealings at 1450ºC and above, whereas in AEZ1200 phase thickening was observed at 1400ºC. The activation energies for coarsening were estimated for both eutectics obtaining a similar value, ~ 300 kJ/mol.

In addition, the crystal orientation of the phases, which behave as single crystals in the as-grown material, appears somewhat scattered after the annealing treatment. The growth directions remained unchanged and are, in all cases,

$[100]_{EAG}//[100]_{ESZ}//[0001]_{Al2O3}$. Although the crystal orientation is not significantly altered by heat treatment for the AEZ eutectics solidified at 25 or 350 mm/h, there could be some reorientation of the ESZ phase in AEZ1200 when annealed, which otherwise shows a strong OR in relation to the Al_2O_3 phase: $(010)_{ESZ}$ // $(0001)_{Al2O3}$ and $(010)_{ESZ}$ // $(10\bar{1}\,0)_{Al2O3}$.

ACKNOWLEDGEMENTS

The authors acknowledge the financial support from the Ministerio de Ciencia e Innovación de España and from the FEDER funds of the European Community under project MAT2009-13979-C03-03. The authors would like to acknowledge the use of Servicio General de Apoyo a la Investigación-SAI,, Universidad de Zaragoza. The authors also thank Dr. J. Y. Pastor and Dr. A. Martín for their experimental support. S. Serrano-Zabaleta thanks the Spanish Government for a grant and M. C. Mesa also thanks the Gobierno de Aragón for a grant.

REFERENCES

[1] Jackson KA, Hunt JD. Lamellar and Rod Eutectic Growth. Trans Metal Soc AIME 1966;236:1129-42.

[2] LLorca J, Orera VM. Directionally-solidified eutectic ceramic oxides. Prog Mat Sci 2006;51:711-809.

[3] Waku Y, Nakagawa N, Wakamoto T, Ohtshubo H, Shimizu K, Kohtoku Y. High-temperature strength and thermal stability of a unidirectionally solidified Al_2O_3/YAG eutectic composite. J Mater Sci 1998;33:1217-25.

[4] Parthasarathy TA, Mah TI, Matson LE. Deformation Behavior of an $Al_2O_3/Y_3Al_5O_{12}$ Eutectic Composite in Comparison with Sapphire and YAG. J Am Ceram Soc 1993;76:29-32.

[5] Pastor JY, Llorca J, Salazar A, Oliete PB, de Francisco I, Peña, JI. Mechanical Properties of Melt-Grown Alumina–Yttrium Aluminum Garnet Eutectics up to 1900 K. J Am Ceram Soc 2005;88:1488-95.

[6] Ramírez-Rico J, Pinto-Gómez AR, Martínez-Fernández J, de Arellano-López AR, Oliete PB, Peña JI, Orera VM. High-temperature plastic behaviour of Al_2O_3–$Y_3Al_5O_{12}$ directionally solidified eutectics. Acta Mater 2006;54:3107-16.

[7] Peña, J. I., M. Larsson, R. I. Merino, I. de Francisco, V. M. Orera, J. Llorca, J. Y. Pastor, A. Martin, and J. Segurado. "Processing, Microstructure and Mechanical Properties of Directionally-Solidified Al_2O_3-$Y_3Al_5O_{12}$-ZrO_2 Ternary Eutectics." J Eur Ceram Soc 2006; 26[15]:3113-21.

[8] Pastor JY, Llorca J, Salazar A, Oliete PB, de Francisco I, Peña JI., Mechanical Properties of Melt-Grown Alumina-Yttrium Aluminium Garnet Eutectics up to 1900K. J Am Ceram Soc 2005;88:1488-95.

[9] Oliete PB, Peña JI, Larrea A, Orera VM, LLorca J, Pastor JY, Martín A, Segurado J. Ultra-High Strength Nanofibrillar Al_2O_3-YAG-YSZ Eutectics. Adv Mater 2007;19: 2313-18.

[10] Yoshikawa A, Hasegawa K, Lee JH, Durbin SD, Epelbaum BM, Yoon DH, et al. Phase identification of $Al_2O_3/RE_3Al_5O_{12}$ and $Al_2O_3/REAlO_3$ (RE=Sm-Lu, Y) eutectics. J Cryst Growth 2000;218:67-73.

[11] Fernandez JM, Sayir A, Farmer SC. High Temperature Creep Deformation of Directionally Solidified $Al_2O_3/Er_3Al_5O_{12}$. Acta Materialia 2003;51[6]:1705-20.

[12] Mazerolles L, Perriere L, Lartigue-Korinek S, Parlier M. Creep Behavior and Related Structural Defects in Al_2O_3-Ln_2O_3 (ZrO_2) Directionally Solidified Eutectics (Ln = Gd, Er, Y). J Eur Ceram Soc 2011;31[7]:1219-25.

[13] Mazerolles L, Perriere L, Lartigue-Korinek S, Piquet N, Parlier M. Microstructures, Crystallography of Interfaces, and Creep Behavior of Melt-Growth Composites. J Eur Ceram Soc 2008;28[12]:2301-8.

[14] Waku Y, Nakagawa N, Wakamoto T, Ohtshubo H, Shimizu K, Kohtoku Y. High-temperature strength and thermal stability of unidirectionally solidified Al_2O_3/YAG eutectic composite. J Mater Sci 1998;33:1217-25.

[15] Nakagawa N, Ohtsubo H, Mitani A, Shimizu K, Waku Y. High temperature strength and thermal stability for melt growth composite. J Eur Ceram Soc 2005;25:1251-7.

[16] Mesa MC, Oliete PB, Larrea A. Microstructural stability at elevated temperatures of directionally solidified Al_2O_3/$Er_3Al_5O_{12}$ eutectic ceramics. J Cryst Growth 2012;360: 119-22.

[17] Park DY, Yang JM, Collins JM. Coarsening of Lamellar Microstructures in Directionally Solidified Yttrium Aluminate/Alumina Eutectic Fiber. J Am Ceram Soc 2001;84 [12]:2991-6.

[18] Matson LE, Hecht N. Microstructural Stability and Mechanical Properties of Directionally Solidified Alumina/YAG Eutectic Monofilaments. J Eur Ceram Soc 1999;19:2487-501.

[19] Waku Y, Sakata S, Mitani A, Shimizu K, Ohtsubo H, Hasebe M. Microstructure and high-temperature strength of Al_2O_3/$Er_3Al_5O_{12}$/ZrO_2 ternary melt growth composite. J Mater Sci 2005;40:711-7.

[20] Oliete PB, Peña JI. Study of the gas inclusions in $Al_2O_3/Y_3Al_5O_{12}$ and $Al_2O_3/Y_3Al_5O_{12}/ZrO_2$ eutectic fibers grown by laser floating zone. J Cryst Growth 2007;304:514-9.

[21] Exner HE, Hougardy HP. In Quantitative Image Analysis of Microstructures, Informationsgesellschaft-Verlag; 1988.

[22] Channel 5. Oxford Instruments HKL. ® HKL Technology 2006. Denmark.

[23] Stegmann H., Waltenberg C., Serrano-Zabaleta S., Larrea A. EBSD analysis of nonconductive samples using in-situ charge compensation. Microscopy and Analysis, *in press*

[24] Wilkinson AJ, Britton TB. Strains, planes, and EBSD in materials science. Materials Today 2012;15;166-76.

[25] Mesa MC, Oliete PB, Larrea A, Orera VM. Directionally Solidified Al_2O_3-$Er_3Al_5O_{12}$-ZrO_2 Eutectic Ceramics with Interpenetrating or Nanofibrillar Microstructure: Residual Stress Analysis. J Am Ceram Soc 2012;95[3]:1138-46.

[26] Yang J-M, Jeng SM, Chang S. Fracture Behaviour of Directionally Solidified $Y_3Al_5O_{12}/Al_2O_3$ Eutectic Fiber. J Am Ceram Soc 1996;79[5]:1218-22.

[27] Graham L D, Kraft RW. Coarsening of eutectic microstructures at elevated temperatures. Trans Met Soc AIME 1966;236:94-102.

[28] Ardell AJ. "Microstructural Stability at Elevated Temperatures," J. Eur. Ceram. Soc. 1999;19:2217-31.

[29] Rylands LM, Wilkes DM, Rainforth WM, Jones H. Coarsening of precipitates and dispersoids in aluminium alloy matrices: a consolidation of the available experimental data. J Mater Sci 1994;29:1895-900.

[30] Lifshitz IM, Slyozov VV. The kinetics of precipitation from supersaturated solid solutions. J Phys Chem Solids 1961;19:35-50.

[31] Speight MV. Growth kinetics of grain-boundary precipitates. Acta Metall 1968;16:133-5.

[32] Ardell AJ. On the coarsening of grain boundary precipitates. Acta Metall 1972;20:601-9.

[33] Iwashita CH, Wei RP. Coersening of grain boundary carbides in a nickel-based ternary alloy during creep. Acta Mater 2000;48:3145-56.

[34] Paladino AE, Kingery WD. Aluminum Ion Diffusion in Aluminum Oxide. J Chem Phys 1962;37[5]:957-62.

[35] Heuer A. H. Oxygen and aluminum diffusion in a-Al_2O_3: How much do we really understand? J Eur Ceram Soc 2008;28:1495-507.

[36] Moya E. G., Moya F., Lesage B., Loudjani M. K. and Grattepain C. Yttrium diffusion in a-alumina single crystal. J Eur Ceram Soc 1998;18:591-4.

[37] Lesage B, Huntz AM. Influence of Chromium and Yttrrium Doping on Transport Phenomena in Monocrystalline Alpha-Alumina. Sol. State Ion 1984;12:243-51.

[38] Reddy KPR, Cooper AR. Oxigen Diffusion in Sapphire. J Am Ceram Soc 1982;65[12]:634-38.

[39] Haneda H, Miyazawa Y, Shirasaki S. Oxigen Diffusion in Single-Crystal Yttrium Aluminum Garnet. J. Cryst. Growth 1984;68:581-88.

[40] Sakaguchi I, Haneda H, Tanaka J, Yanagitani T. Effect of Composition on the Oxygen Tracer Diffusion in Transparent Yttrium Aluminum Garnet (YAG) Ceramics. J Am Ceram Soc 1996;79[6]:1627-32.

[41] Bates JL, Garnier JE. Electrical Conductivity of $MgA_{l2}O_4$ and $Y_3Al_5O_{12}$. Jam Ceram Soc 1981;64[10]:C-138-41.

[42] Doremus RH. Diffusion in alumina. J. Appl. Phys. 2006;100:101301-1-16.

[43] Oeldgart C, Anderson J, Heinrich JG, Messing GL. Sintering, microstructure and mechanical properties of Al_2O_3-Y_2O_3-ZrO_2 (AYZ) eutectic composition ceramic microcomposites. J Eur Ceram Soc 2010;30:649-56.

[44] Ramirez-Rico J, J., de Arellano-Lopez AR, Martinez-Fernandez J, Pena JI, Larrea A. Crystallographic Texture in Al_2O_3-ZrO_2 (Y_2O_3) Directionally Solidified Eutectics. Journal of the European Ceramic Society 2008;28[14]:2681-86.

[45] Larrea A, Laguna-Bercero MA., Pena JI., Merino RI, Orera VM. Orientation Relationship and Interfaces in Ni and Co-Ysz Cermets Prepared from Directionally Solidified Eutectics. Central European Journal of Physics 2009;7[2]:242-50.

[46] Mazerolles L, Nicolas Piquet12, no. 7 (2008): 499-505.

[47] Laguna-Bercero MA, Larrea A, Merino RI, Peña JI, Orera VM. Stability of channeled Ni-YSZ Cermets produced from self-assembled NiO-YSZ directionally solidified eutectics. J Am Ceram Soc 2005;88;3215-17.

FIGURE CAPTIONS

Figure 1: Back-scattered scanning electron micrographs of the transverse cross-section of (a) AEZ25, (b) AEZ350 and (c) AEZ1200 as-grown, (d) AEZ25, (e) AEZ350 and (f) AEZ1200 after annealing at 1450ºC for 100h in air, and (g) AEZ25 (h) AEZ350 and (i) AEZ1200 after annealing at 1600ºC for 100h in air.

Figure 2: Back-scattered scanning electron micrographs of the longitudinal cross-section of (a) AEZ1200 as-grown and (b) AEZ1200 after annealing at 1600ºC for 100h in air.

Figure 3: Interspacing, λ, as a function of the annealing time, t, for (a) AEZ350 and (b) AEZ1200.

Figure 4: Surface density, S_v, as a function of the annealing time, t, for the transverse cross-section of (a) AEZ350 and (b) AEZ1200.

Figure 5: Orientation map of the as-grown AEZ25 sample. Pixels of the same colour indicate areas with identical orientation. Only three hues can be distinguished since each phase behaves as a single crystal: the darkest (black) areas correspond to Al_2O_3, grey (violet) areas to EAG, and light grey (orange) to ESZ.

Figure 6: Experimental pole figures of the as-grown AEZ25 for (a) EAG, (b) ESZ and (c) Al_2O_3. Growth directions are indicated by round markers $[100]_{EAG}//[100]_{ESZ}//[0001]_{Al2O3}$. Possible interfacial planes are indicated by square markers.

Figure 7: Orientation map of the as-grown AEZ solidified at 350 mm/h. The darkest (black) areas correspond to Al_2O_3, grey (violet) areas to EAG, and light grey (green) to ESZ. The appearance of several shades of yellowish green indicates there is some scattering in the ESZ crystal orientation.

Figure 8: Orientation map of the AEZ sample solidified at 1200 mm/h (a) as-grown and (b) after 100 h of annealing at 1600 °C. The darkest (black) areas correspond to Al_2O_3, grey (ultramarine blue) areas to EAG, and light grey (green and light blue) to ESZ.

Table 1: Interspacing, λ, of the AEZ eutectics as-grown and after annealing at 1600ºC for 100h.

	λ (μm)		
	AEZ25	AEZ350	AEZ1200
As grown	4.8±0.5	0.8±0.1	0.3±0.03
1600ºC 100h	4.8±0.3	2.1±0.4	2.1±0.3

Table 2: Surface density, S_v, of the AEZ eutectics as-grown and after annealing at 1600ºC for 100h.

	S_v (μm^{-1})					
	AEZ25		AEZ350		AEZ1200	
	Transverse	Longitudinal	Transverse	Longitudinal	Transverse	Longitudinal
As grown	1.8±0.2	1.3±0.1	8.0±1.1	5.7±1.0	16.3±2.0	9.9±1.2
1600ºC 100h	1.5±0.2	1.1±0.1	2.1±0.2	1.7±0.2	1.7±0.2	1.6±0.2

Figure
Click here to download high resolution image

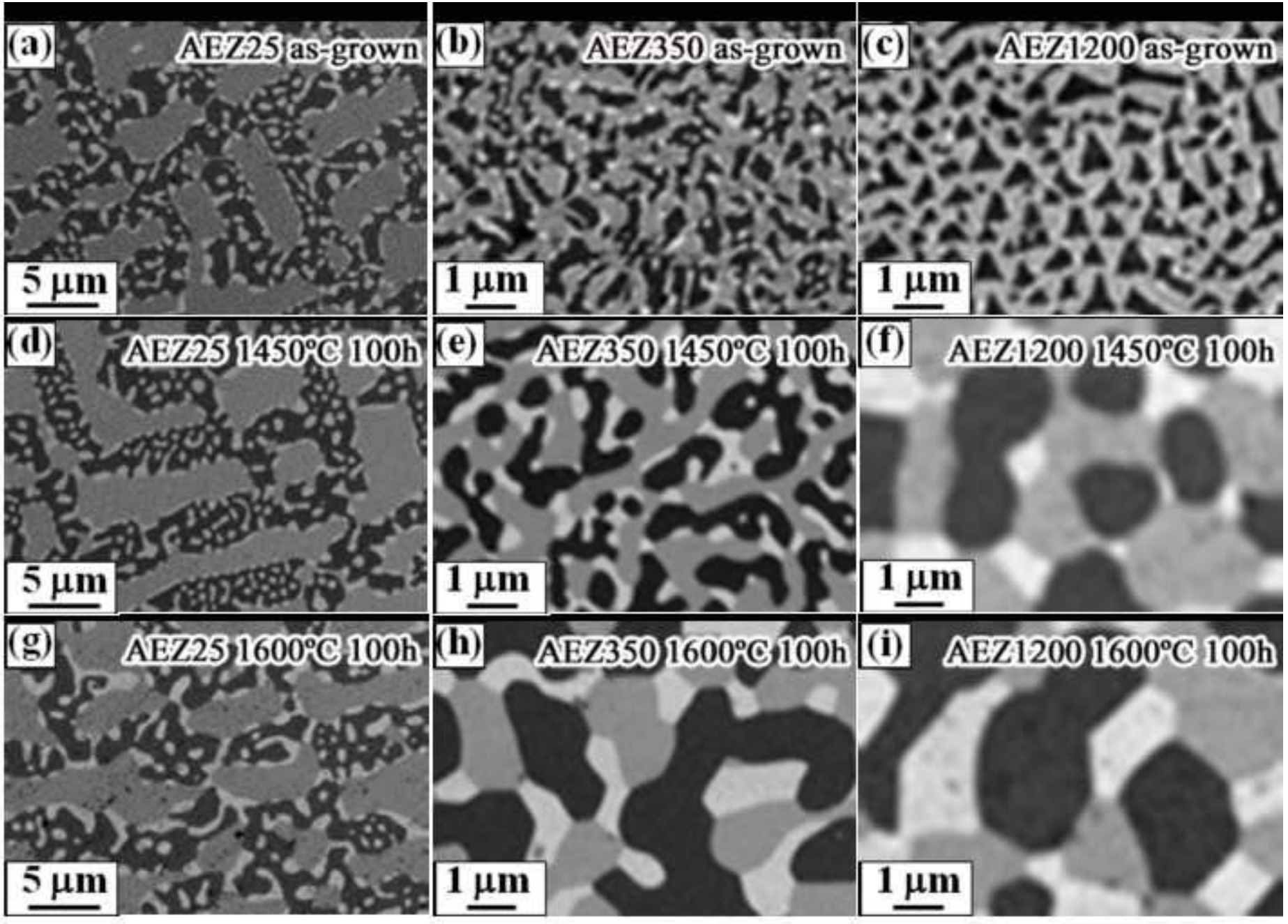

Figure 1

Figure
Click here to download high resolution image

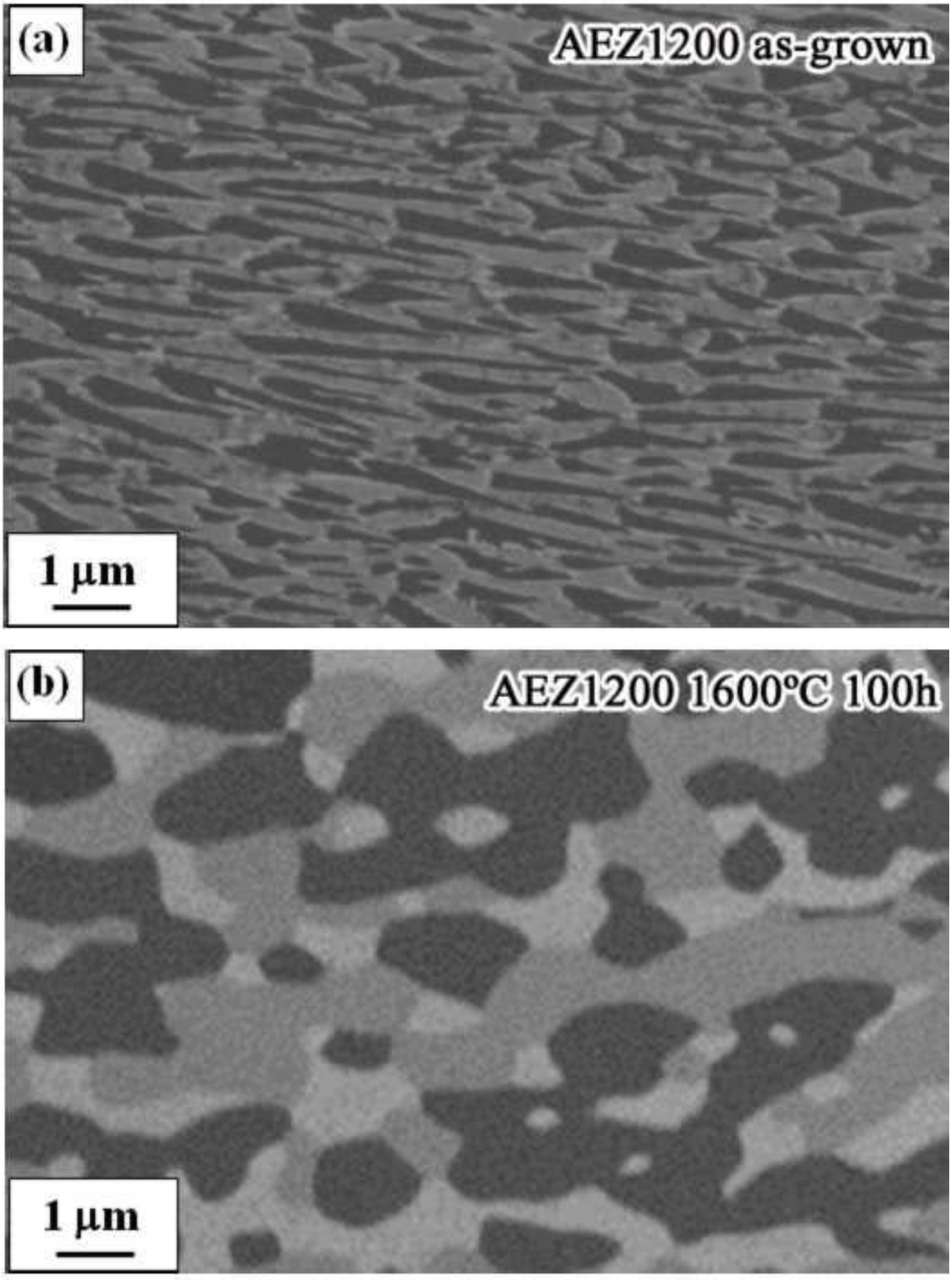

Figure 2

Figure
Click here to download high resolution image

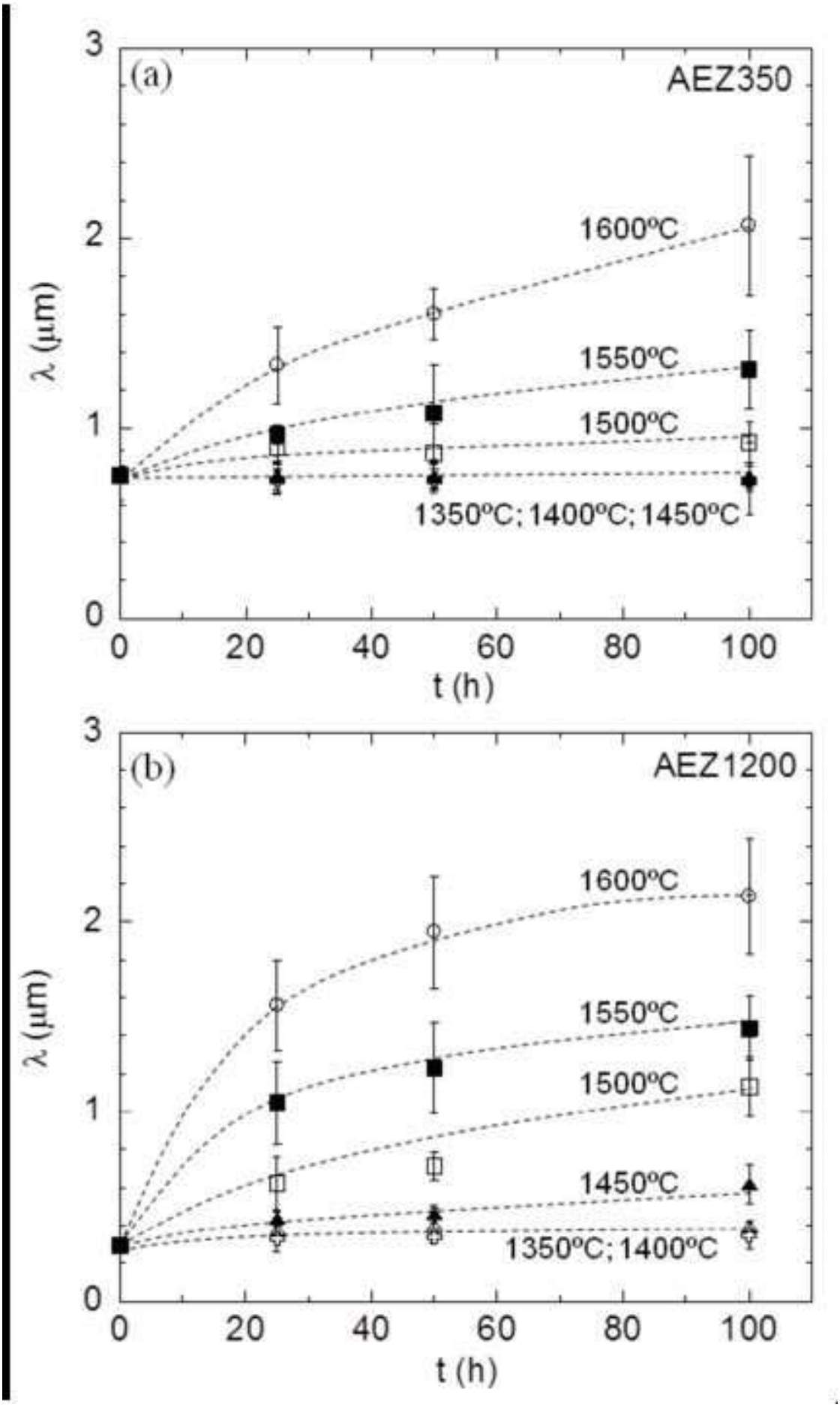

Figure 3

Figure
Click here to download high resolution image

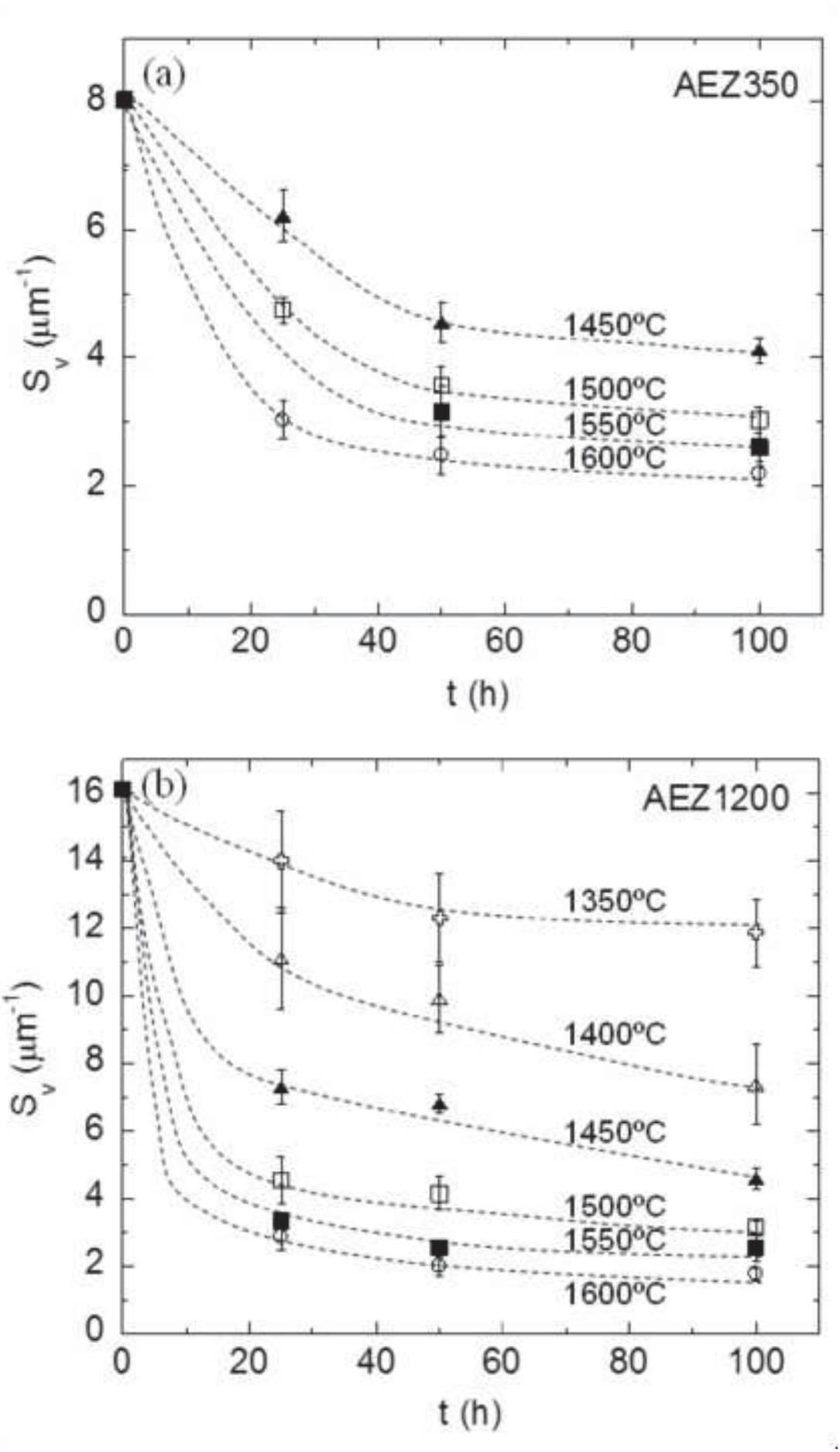

Figure 4

Figure 5

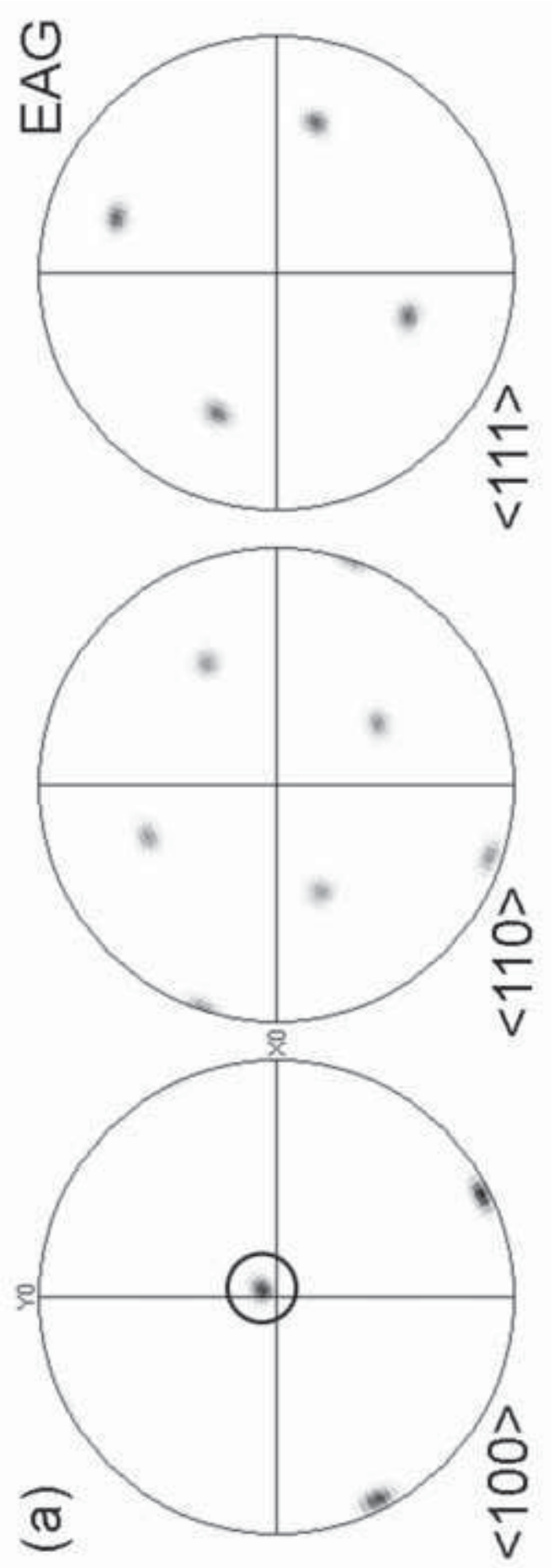

Figure 6a

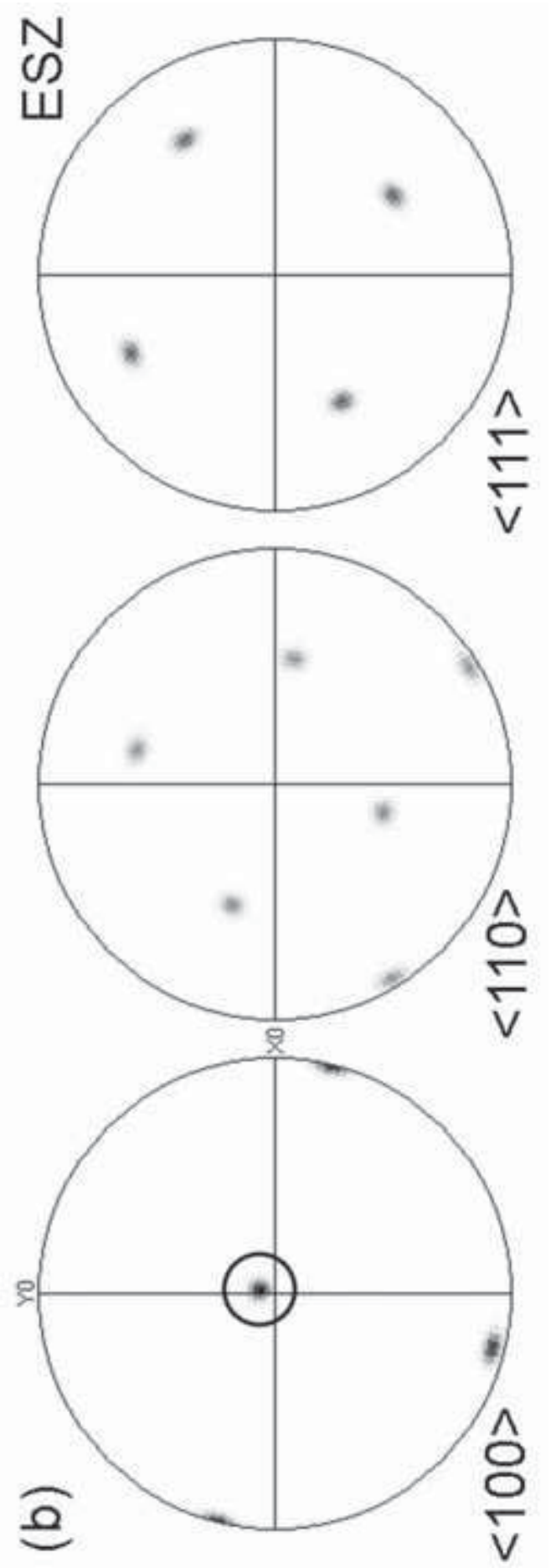

Figure 6b

Figure
Click here to download high resolution image

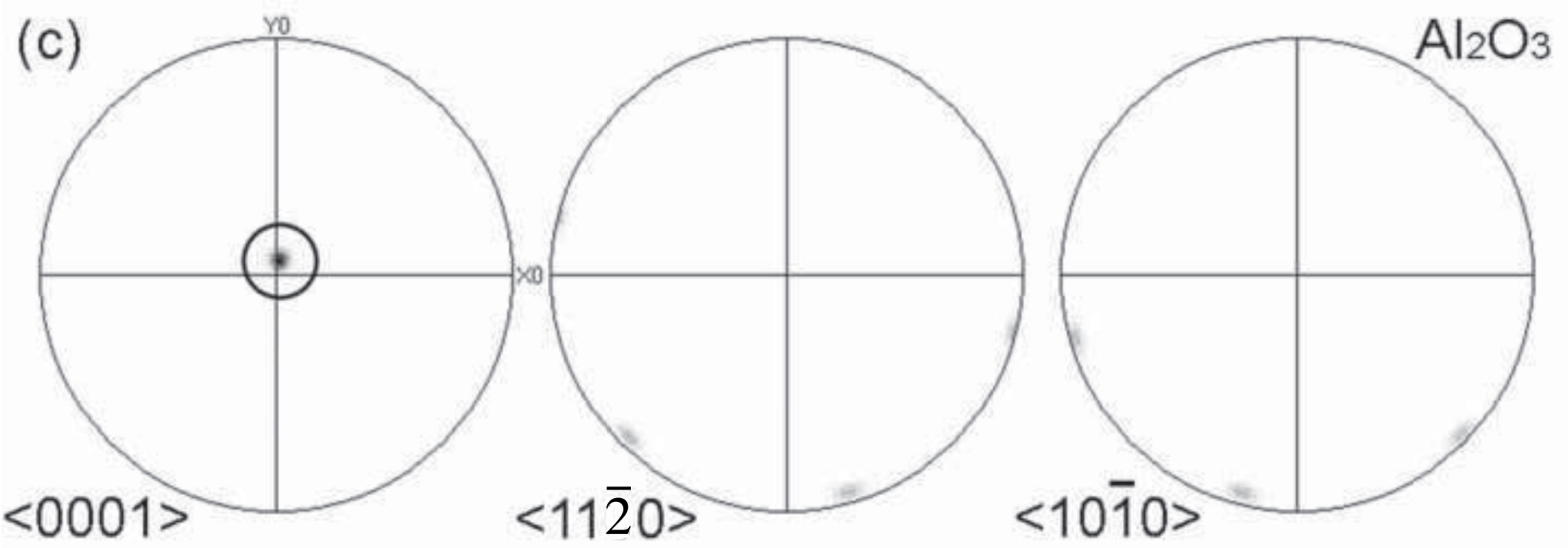

Figure 6c

Figure 7

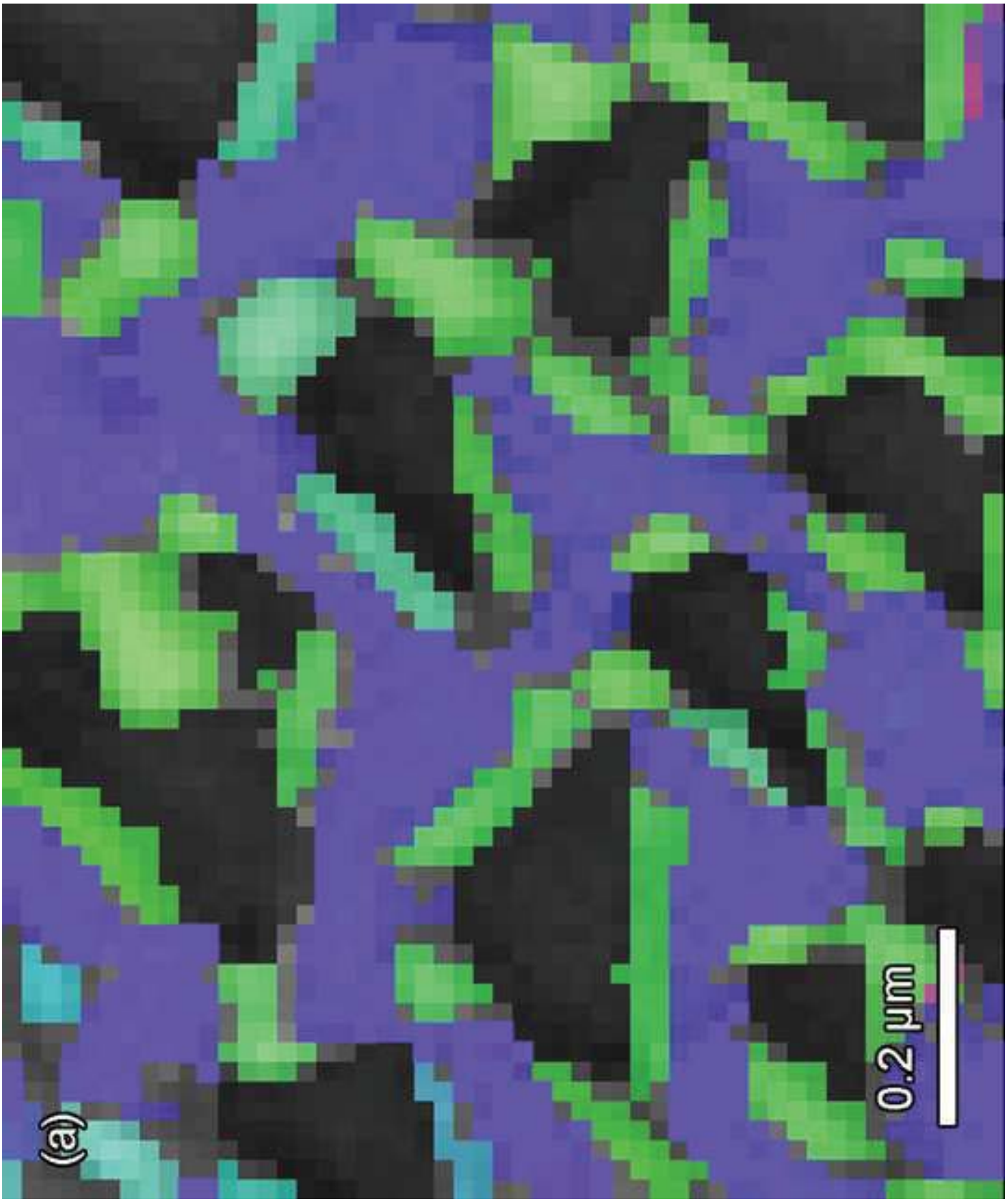

Figure 8a

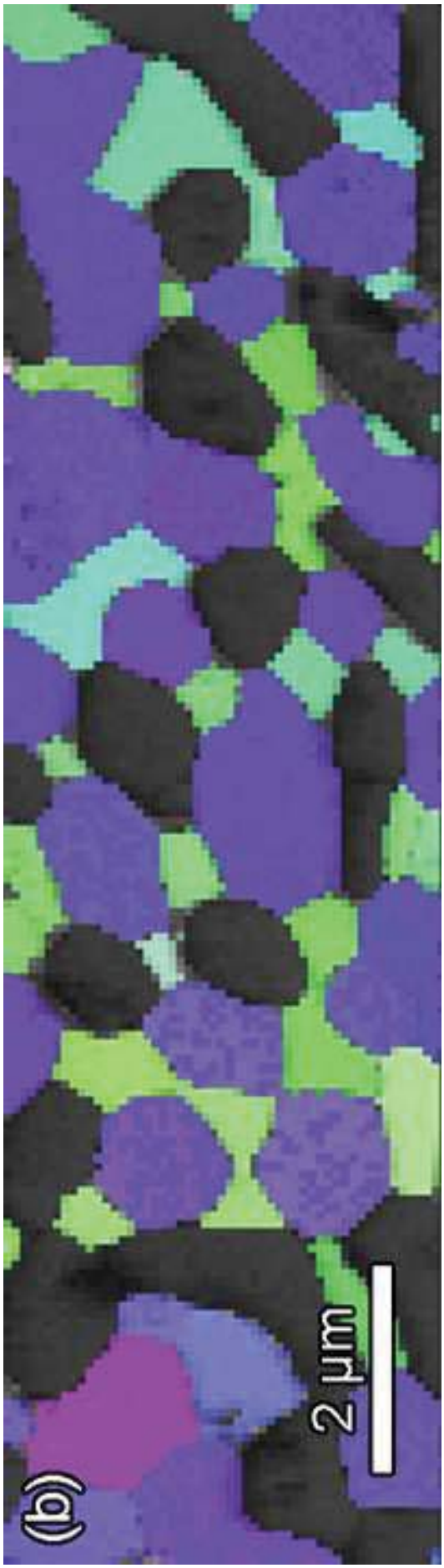

Figure 8b